17th Brazilian Congress of Thermal Sciences and Engineering
November 25th-28th, 2018, Águas de Lindóia, SP, Brazil

ENCIT-2018-0463
NUMERICAL INVESTIGATION OF THE INFLUENCE OF THE FLOW DIMENSIONLESS PARAMETERS ON THE HEAT TRANSFER OF A VISCOPLASTIC FLUID

Dulles Araujo Gomes
Luiz Paulo Borges Miranda
Daniel Dall'Onder dos Santos
Federal University of Uberlândia, Av. João Naves de Ávila 2121, Uberlândia, MG, 38408-100, Brazil
dulles.gomes@gmail.com
luiz.miranda@ufu.br
dallonder@ufu.br

Abstract. *There is a significant use of non-Newtonian fluids in the industry, therefore, a study of their behavior is necessary in order to avoid errors in projects. Some of these fluids presents yield stress characteristics – the fluid must overpass a certain amount of stress to actually flow. This is called the viscoplastic behavior. This work presents a study on the influence of the rheological dimensionless quantities of a viscoplastic fluid on heat transfer. The mechanical model is approximated in a numerical simulation code called NNFEM, using the SMD viscoplastic model. The NNFEM code is based on the Galerkin least-squares methodology and it is validated in several works in the literature. The Reynolds number and the plastic number are varied individually in order to analyze the impact of these parameters on the ability to transfer heat along the flow. The adopted geometry is a planar channel which has an expansion followed by an abrupt contraction. The channel walls are kept insulated and the heat transfer occurs only at the expansion-contraction walls. The obtained results have physical meaning and are in accordance with the ones found in the literature.*

Keywords: *Viscoplastic Behavior; rheological properties; SMD model; heat transfer; expansion and abrupt contraction*

1. INTRODUCTION

It is recognized that many multiphase and / or structured fluids such as foams, emulsions and suspensions found in a variety of engineering applications exhibit viscoplastic behavior. Some typical examples are: processed foods and chocolates; toiletries and cosmetics; drilling muds, lubricants and greases; construction materials; among others (Nirmalkar *et al*., 2014). In these applications, heat transfer and pressure drop are important parameters, as they are used to predict the flow behavior and to estimate the energy necessary for heating and transportation. Frigaard *et al*. (2017) reviews the usage of yield stress fluid flows in the oil and gas industry.

The heat transfer in viscoplastic systems differs significantly from that in Newtonian fluids or in purely viscous fluids without a yield stress: the coexistence of the fluid-like (yielded) and solid-like (unyielded) regions in the flow affect the characteristics of the flow and the heat transfer mechanisms. To understand this phenomenon, several studies have been developed, for different configurations: Turan *et al.* (2011) simulated a two-dimensional steady-state natural convection in rectangular enclosures with differentially heated side walls in a range of different aspect ratios of the enclosure, a range of Rayleigh numbers, and a range of Bingham numbers too. Raja *et al*. (2015) investigated the flow of a Bingham plastic fluid past a two-dimensional heated flat plate over a range of Reynolds numbers, Prandtl numbers, and Bingham numbers. Nirmalkar *et al.* (2014) solved numerically the equations of motion and energy for the laminar free convection heat transfer from a horizontal heated cylinder to Bingham plastic fluids over the range of conditions as: Rayleigh number, Prandtl number, and Bingham number. Shyam and Chhabra (2013) have developed a numerical solution for the momentum and heat transfer characteristics of a heated cylinder of square cross-section immersed in a streaming Bingham plastic medium, imposing the plastic Reynolds number, the Prandtl number, and the Bingham number. Gupta *et al.* (2017a) analyzed the laminar forced convection momentum and heat transfer characteristics of a circular disk positioned inside a flow of Bingham plastic fluid and oriented normal to the flow. The disk was modelled by two different conditions: a constant flux and a constant temperature condition. Both conditions were analyzed for a range of Reynolds number, Prandtl number, Bingham number, and for different ratios thickness-to-diameter of the disk.

The mentioned studies highlight a positive dependence of the Nusselt number with the Reynolds number for different geometries. These results are in accordance with the results obtained in the present work.

Although not directly related to this work, some authors have also discussed the effects of the temperature over the rheological properties, and how they affect the flow and the heat transfer. Soares *et al.* (1999) numerically analyzed the

heat transfer in the entrance-region of tubes for Herschel-Bulkley fluid flows. The mechanical model considered two different boundary conditions: constant wall heat flux and constant wall temperature to investigate the effects of temperature-dependent properties. Nouar *et al.* (1995) present a numerical analysis of the laminar forced convection in a cylindrical duct for a thermo-dependent Herschel-Bulkley fluid considering constant wall heat flux and constant wall temperature. The governing equations were solved using the finite difference method assuming all fluid properties constant except the consistency index constant. The authors obtained correlations for the local Nusselt number and the pressure gradient considering the temperature-dependent characteristic of the fluid. Gupta *et al.* (2017b) analyzed the effects of viscous dissipation and the temperature-dependent viscosity on the Nusselt number modelling an isothermal spheroid immersed in a Bingham plastic fluid.

The model adopted in this work to model the viscoplastic behavior is the one proposed by de Souza Mendes and Dutra (2004). This model is continuous and has continuous derivatives, making it more convenient for numerical simulation and curve fitting procedure. The qualitative behavior is the same as in the most of the viscoplastic fluids of interest: a high viscosity plateau for low stress, followed by a sharp drop in the viscosity level and then a power-law region (de Souza Mendes and Dutra, 2004). In order to study the influence of the rheological dimensionless properties related to the fluid-flow interactions of viscoplastic fluids in the heat transfer, two parameters have been chosen to be analyzed: the Reynolds number and the plastic number. Each one was varied individually, so its influence on the heat transfer can be identified.

The software used to simulate the flow conditions fluid is known as NNFEM, which is an open source software and has been employed in several non-Newtonian fluid flow studies. The numerical code is based on the Galerkin Least Squares finite element methodology.

2. METHODOLOGY

2.1 Geometry and boundary conditions

The flow is along a planar channel, following the dimensions shown in Fig. 1. The ratio between dimension H2 (cavity height) and dimension H1 (channel height) is equal to 6.3. The ratio of the length of the cavity (L2) to the height of the cavity (H2) is equal to 1 and the ratio of the length L1 (length of the channel) and H1 is equal to 16.85. Thus, the analyzed domain has a length of 40 units. In the works of de Souza Mendes *et al.* (2007) and Hermany, (2012) a similar, but axisymmetric, geometry is found.

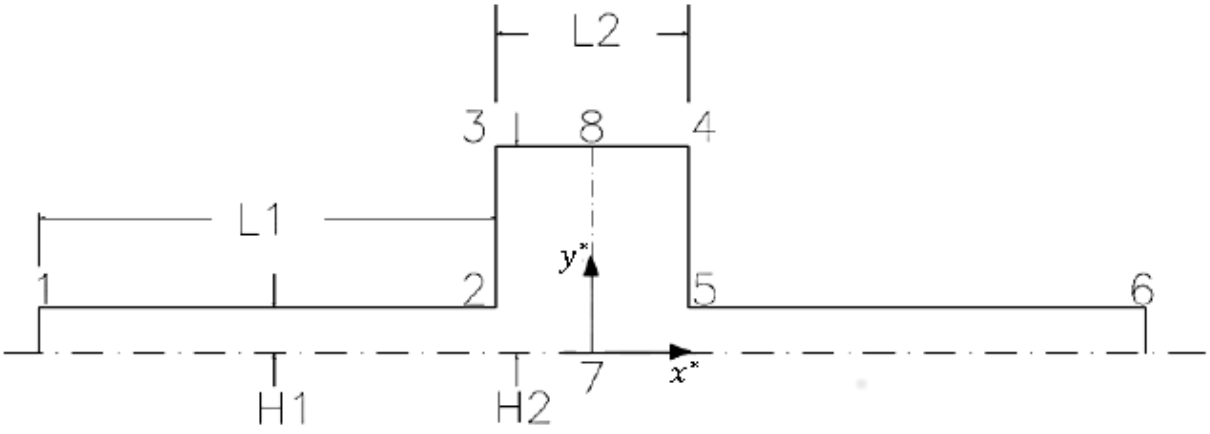

Figure 1. Geometry of the planar channel.

To reduce the numerical effort, only half geometry is simulated (the symmetry line is at y^*=0, with imposed $\mathbf{u}$=0 and $\boldsymbol{\tau}_{xy}$=0). The velocity boundary conditions were impermeability and no-slip on the channel and cavity walls, zero vertical velocity at inlet and outlet and a flat horizontal velocity profile at the inlet. The symmetry and channel walls were considered thermally insulated. The fluid dimensionless temperature at the inlet is equal to 0 and at the cavity walls is equal to 1.

The mesh independence procedure was performed through a stress analysis in the cross-section at the center of the expansion-contraction, for each mesh refinement. The selected mesh has 5200 finite elements. In general, this mesh showed an error less than 1% when compared to more refined meshes. More information can be found in Santos *et al.* (2013). The employed mesh is shown in Fig. 2.

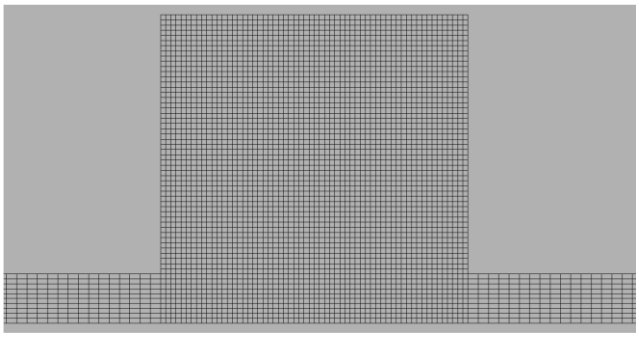

Figure 2. Detail of the central region of the mesh used for the numerical simulations.

2.2 Mechanical model

The fluid is assumed as incompressible, and the continuity, momentum balance and energy balance can be expressed as, respectively:

$$\mathrm{div}(\mathbf{u}) = 0 \tag{1}$$

$$\rho(\nabla \mathbf{u})\mathbf{u} = -\nabla p + \mathrm{div}(\boldsymbol{\tau}) \tag{2}$$

$$\rho c_p(\nabla T)\mathbf{u} = \kappa \nabla^2 T \tag{3}$$

where **u** is the velocity vector, ρ is the specific mass of the fluid, p is the hydrostatic pressure, c_p is the fluid specific heat, T is the temperature and κ is the thermal conductivity. c_p and κ are considered constants. $\boldsymbol{\tau}$ is the extra-stress tensor, and it is defined by the constitutive equation, as follows:

$$\boldsymbol{\tau} = 2\,\eta(\dot{\gamma})\mathbf{D}(\mathbf{u}) \tag{4}$$

D(**u**), $\eta(\dot{\gamma})$ and the shear rate $\dot{\gamma}$ are defined as:

$$\mathbf{D}(\mathbf{u}) = \frac{1}{2}\left(\nabla \mathbf{u} + \nabla \mathbf{u}^T\right) \tag{5}$$

$$\eta(\dot{\gamma}) = \left(1 - \exp\left(\frac{-\eta_0}{\tau_0}\dot{\gamma}\right)\right)\left(\frac{\tau_0}{\dot{\gamma}} + K\dot{\gamma}^{n-1}\right) + \eta_\infty \tag{6}$$

$$\dot{\boldsymbol{\gamma}} = \sqrt{2\,\mathrm{tr}\,\mathbf{D}(\mathbf{u})^2} \tag{7}$$

where η_0 and η_∞ are, respectively, the viscosities for very low and high values of the shear rate $\dot{\gamma}$, τ_0 is the yield stress limit of the material, K is the consistency index, n is the power-law index, which controls the shear-thinning of the fluid when the material starts to flow. Equation (6) represent the SMD model, and shows that $\eta(\dot{\gamma})$ is function of the shear rate, but it is independent of the temperature.

2.3 Dimensionless groups of interest

Due to the viscoplastic nature of this system, the classical dimensionless groups found in the literature groups must be adapted, as shown by Thompson and Soares, (2016). In this work, the dimensionless groups of interest are: the Reynolds number, the Prandtl number, the jump number, the plastic number and the Nusselt number.

The expressions for the Reynolds number (*Re*) and the Prandtl number (*Pr*) used in this work are:

$$\mathrm{Re} = \frac{\rho V^2}{\tau_0 + K\left(\frac{V_c}{L_c}\right)^n + \eta_\infty\left(\frac{V_c}{L_c}\right)} \tag{8}$$

$$\frac{1}{\mathrm{Pr}} = \left[\frac{K\left(\frac{V_c}{L_c}\right)^n + \eta_\infty\left(\frac{V_c}{L_c}\right)}{\tau_0 + K\left(\frac{V_c}{L_c}\right)^n + \eta_\infty\left(\frac{V_c}{L_c}\right)}\right]\left[\frac{\rho\alpha}{K\left(\frac{V_c}{L_c}\right)^{n-1} + \eta_\infty}\right] \tag{9}$$

where α is the thermal diffusivity, *Vc* and *Lc* are the characteristic velocity and the characteristic length, respectively taken as the value of the velocity at the inlet and the channel height (*H1*).

The jump number (*J*) is an adimensional group proposed by de Souza Mendes, (2007), and its expression is:

$$J = \frac{\eta_0\dot{\gamma}}{\tau_0} - 1 \tag{10}$$

The adopted expression of the plastic number (*Pl*) can be found in Thompson and Soares, (2016), and it can be defined as:

$$Pl = \frac{\tau_0}{\tau_0 + K\left(\frac{V_c}{L_c}\right)^n + \eta_\infty\left(\frac{V_c}{L_c}\right)} \tag{11}$$

The Nusselt number (*Nu*) and average Nusselt ($\overline{Nu}$) were calculated as described by Santos and Machado, (2015).

As already stated, the present work analyzed two different parameters individually, so the Prandtl number and the jump number values will be fixed in 14 and 10^4, respectively. The characteristic length does not vary, since the geometry of the planar channel will remain the same during this study, and it is equal to the channel height. The value of η_∞ and *n* are also kept constant, equal to 10^{-2} Pa·s and 0.5 respectively.

3. PRELIMINARY RESULTS

3.1 Influence of Reynolds number

Figure 3 shows the temperature isobands, with Reynolds number ranging from 1 to 40. In this condition the plastic number, Prandtl number, jump number and power-law index assumed values equal to 0.411, 14, 10^4, 0.5, respectively.

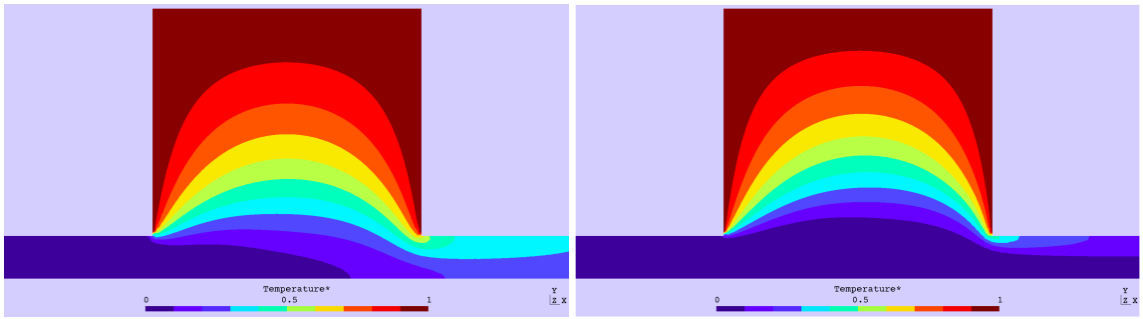

(a) (b)

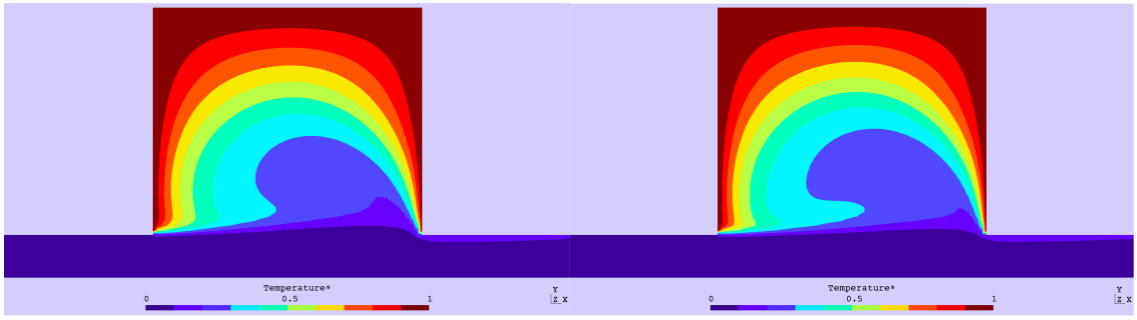

(c) (d)

Figure 3. Temperature zones for different Reynolds number (a) Re = 1; (b) Re = 5; (c) Re = 35; (d) Re = 40.

In Fig. 3 it is possible to observe that for Re = 1 the fluid downstream of the cavity suffers a great influence of the temperature of the fluid inside the cavity, and this phenomenon decreases as the Reynolds increases. Inside the cavity, for low Reynolds numbers, the temperature layers show a gradual increase of the temperature towards the wall of the cavity, but between Re = 20 and Re = 25 there is a disturbance in the flow that generates perturbations in the temperature layers. The perturbation in the temperature field is induced by the presence of a vortex within the cavity which has its intensity increased with increasing *Re*. The Reynolds number can be interpreted as the ratio of the forces of inertia by the viscous forces. Thus, if *Re* = 1, the inertial forces have the same magnitude as the viscous forces, and for Re> 1 the inertial forces prevail. For low Reynolds, the viscous forces are more significant, and they allow more interaction between the fluid in the channel and the fluid inside the cavity. Therefore, lower *Re* numbers increase the regions of the channel affected by the gradient of temperature. When the *Re* numbers increases, the inertial forces increase its influence, and the flow starts to lose his capacity of interaction with the cavity. But between Re = 20 and Re = 25 a secondary flow is generated, and this vortex forces the interaction between the fluid in the channel and the fluid inside the cavity, increasing the heat transfer.

Figure 4 shows the unyielded regions for the analyzed flows. When Re = 1, it is possible to identify a symmetry, however, as the inertial forces increase over the viscous forces, this symmetry disappears, and the rigid zone profiles assume other configurations. As observed in the temperature field, between Re = 20 and Re = 25 a secondary flow arises within the cavity and the presence of this vortex induces the unyielded regions observed in Fig. 10 (c). Next to the center of the vortex the relative velocities between the fluid particles are low and induce a unyielded region in this zone. As the Reynolds number increases, the dimensions of the vortex and its central unyielded region increase too. However, with the increase of the zone of influence of the secondary flow, the upper unyielded region tends to be decreased.

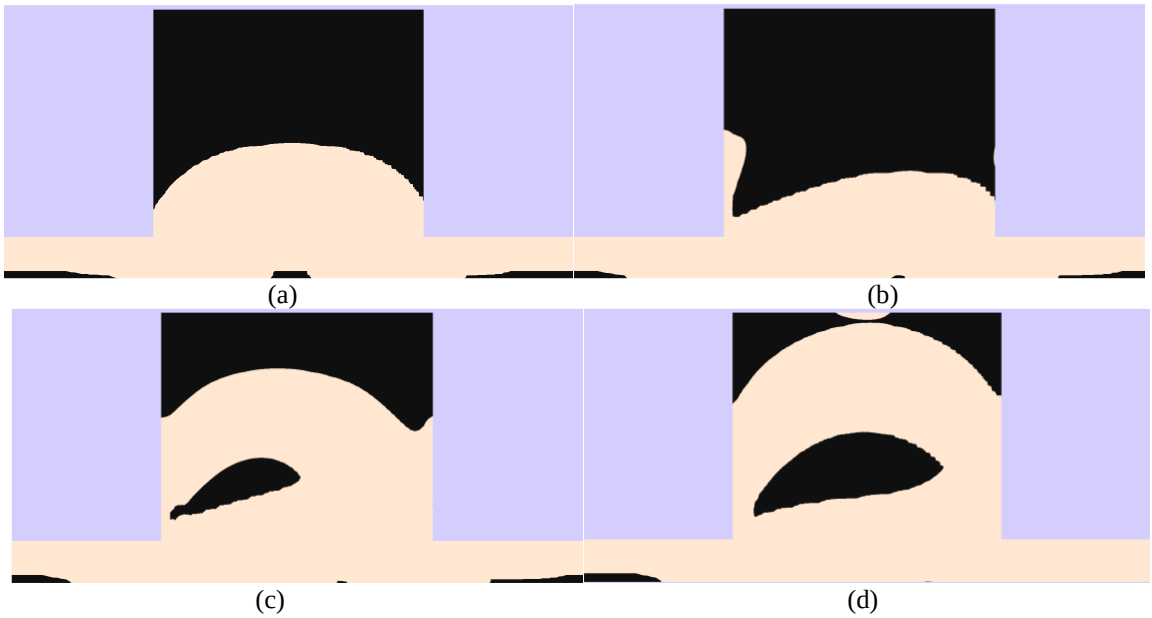

(a) (b)

(c) (d)

Figure 4. Yield zones for (a) Re = 1; (b) Re = 20; (c) Re = 25; (d) Re = 40.

Figure 5 shows the temperature of the fluid along the vertical axis y^*, at x^* = 0. The only simulated value where that the temperature is different from the inlet temperature is when *Re* = 1. As discussed above, the temperature field for

Re = 1 has its most constant growth due the heat transfer induced by influence of the viscous forces, which allows more interaction between the fluid of the channel and the fluid inside the cavity. With the increase of *Re*, the heat exchange between the channel fluid and the cavity fluid decreases, which causes the temperature to raise more sharply when y^* is approximately equal to the main channel height (*H1*=1). With the arising of the secondary flow, the temperature rises rapidly when it enters the zone of influence of the vortex, but once inside the vortex, the temperature tends to stabilize. Once the boundary of the vortex is achieved, the temperature starts to increase once again.

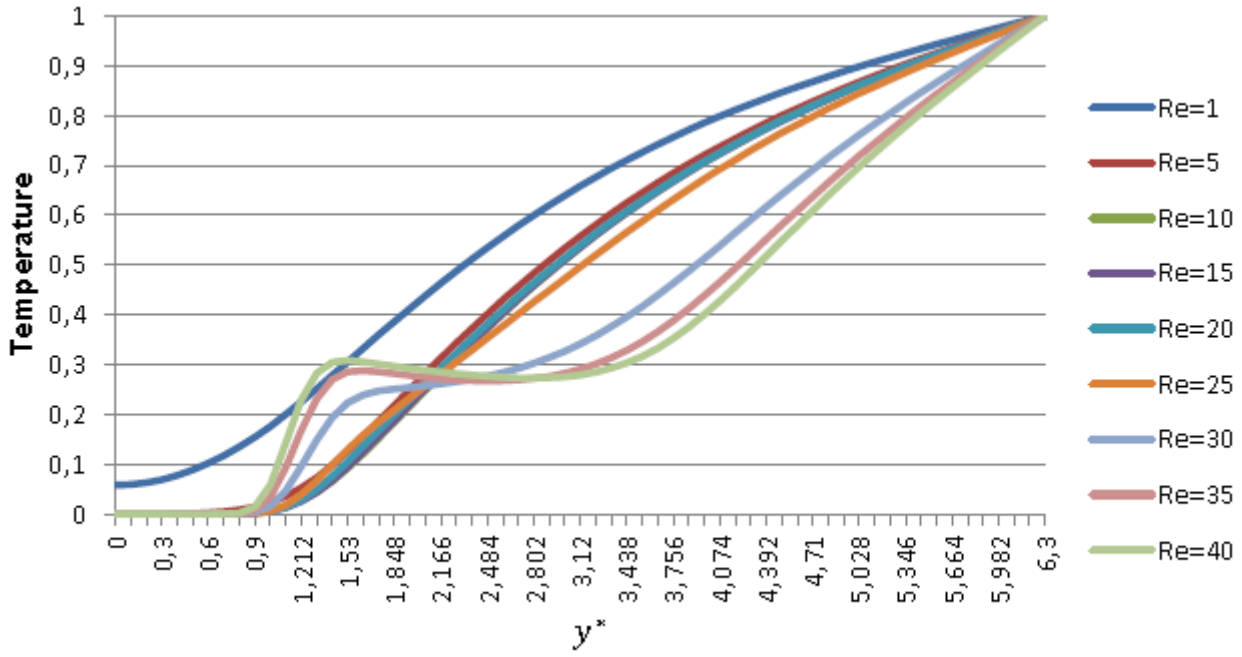

Figure 5. Temperature along the axis y^* for different *Re*

Figure 6 compares the temperature of the fluid downstream of the cavity at the channel wall. Since the walls are thermally insulated, the fluid tends to exchange heat with itself and ends up homogenizing the flow temperature at downstream of the cavity.

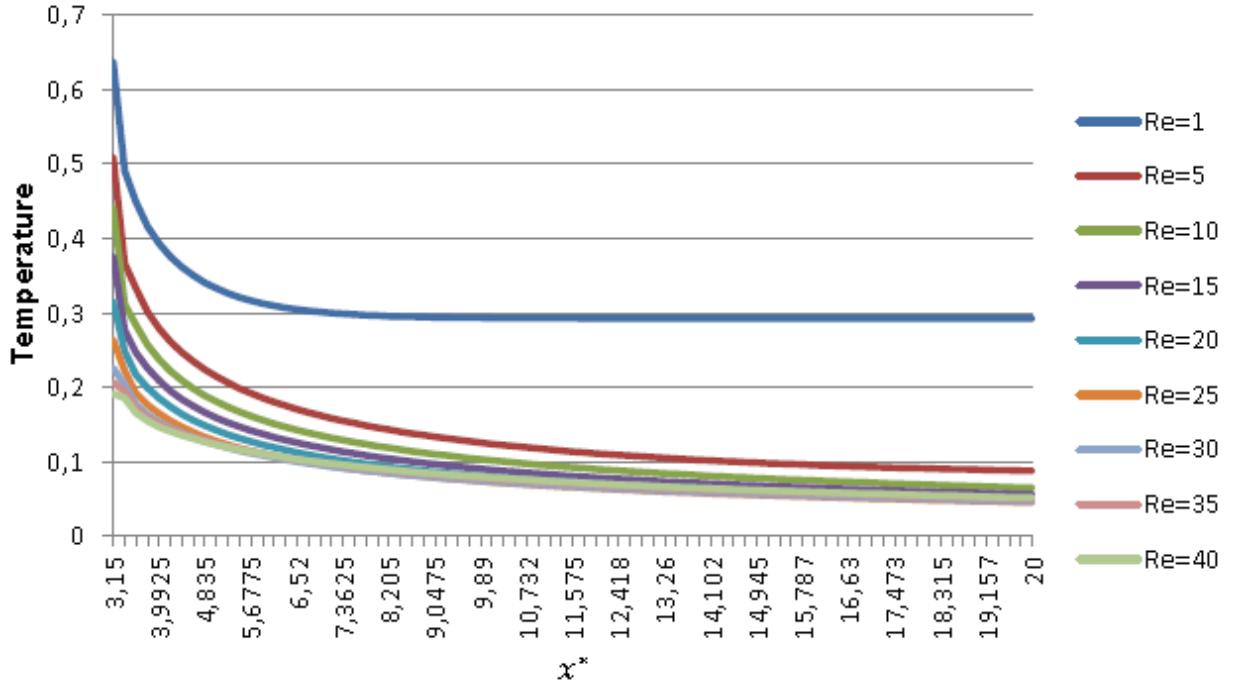

Figure 6. Temperature along the channel wall downstream the cavity varying the Reynolds number.

The Nusselt number expresses the ratio between the heat exchange by convection and the heat exchange by conduction. Figure 7 shows how the average Nusselt number, evaluated at the cavity's wall perimeter, varies as a function of the Reynolds number. A general aspect of the curve suggests that the increase of Re generates an increase of Nu, this information can be associated with the size of the unyielded region in each flow, since in these zones the thermal exchange by conduction is predominant. In other words: the greater the unyielded region, smaller the Nu. In Fig. 4 it is possible to identify the decrease of the unyielded region as the Reynolds number increases. The increase of the inertia forces over the viscous forces tends to decrease the unyielded region, and increase the average Nusselt number. The development of a secondary flow for $Re > 25$ accelerates the decrease of the unyielded region, and thus favors the increase of the Nu.

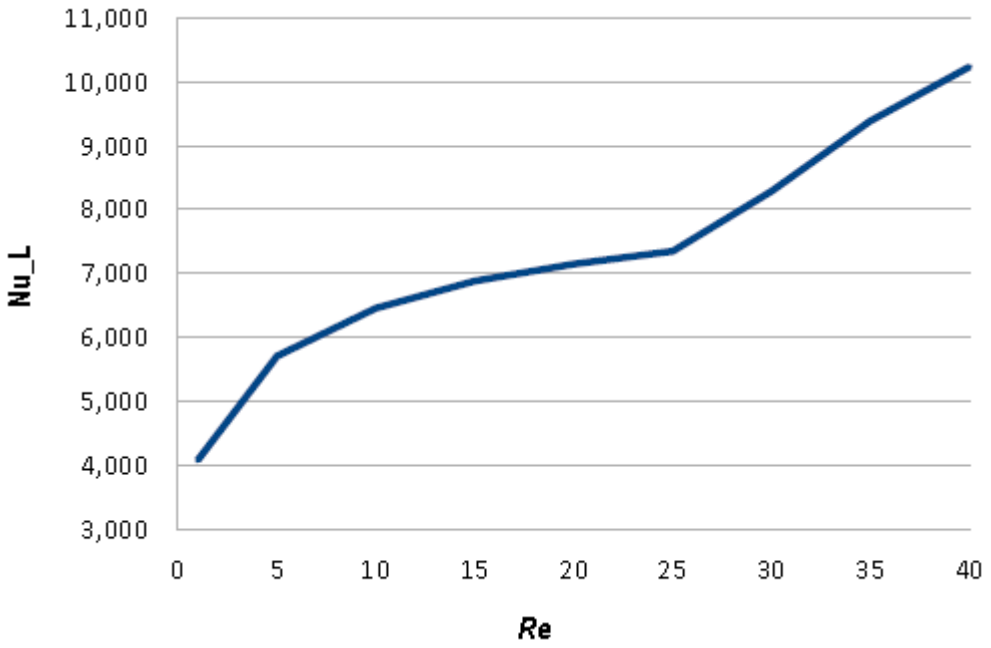

Figure 7. average Nusselt number in the perimeter of the cavity as a function of Reynolds number.

3.2 Influence of the plastic number

The flow studied in this section has only the variation of the plastic number; the Reynolds number is fixed at 24.87, the Prandtl number is 14, the jump number remains fixed and equal to 10^4, and the power-law index is fixed in 0.5.

The plastic number is subjected to a variation ranging from 0.083 to 0.727. A low plastic number means that the fluid only needs a small amount of stress to be able to flow. A plastic number close to 1 means that the fluid has a strong viscoplastic characteristic, with a high yield stress, which facilitates the appearance of apparently unyielded areas.

Figure 8 shows the temperature isobands for different values of the plastic number. Due to the value of the Reynolds number fixed in these simulations a low interaction of the fluid inside the cavity and the fluid of the channel is expected. Contrary to what was observed in the previous parameter, low plastic numbers generate perturbations in the thermal zones, and the increase of the plastic number tends to organize them. This phenomenon happens due to the fact that for low plastic numbers, the yield stress is low too, and the fluid has more ease to flow, therefore the cavity flow is more influenced by main flow. At $Pl = 0.083$, the fluid has low influence of its viscoplasticity, which allows the main flow to find greater ease to induce a secondary flow inside the cavity, and thus producing a vortex that disorganizes the temperature layers using the same mechanisms mentioned in the section above. The ease of fluid flow and the size of the vortex formed within the cavity, observed by the semicircle created by the temperature layer of Fig. 8 (a), drives parts of fluid out of the cavity, causing a larger temperature gradient in the downstream of the cavity. As the plastic number increases, the yield stress also increases, and the flow tends to show more rigid zones. This event diminishes the action of the secondary flow and tends to diminish the effects discussed previously, until neutralizing them.

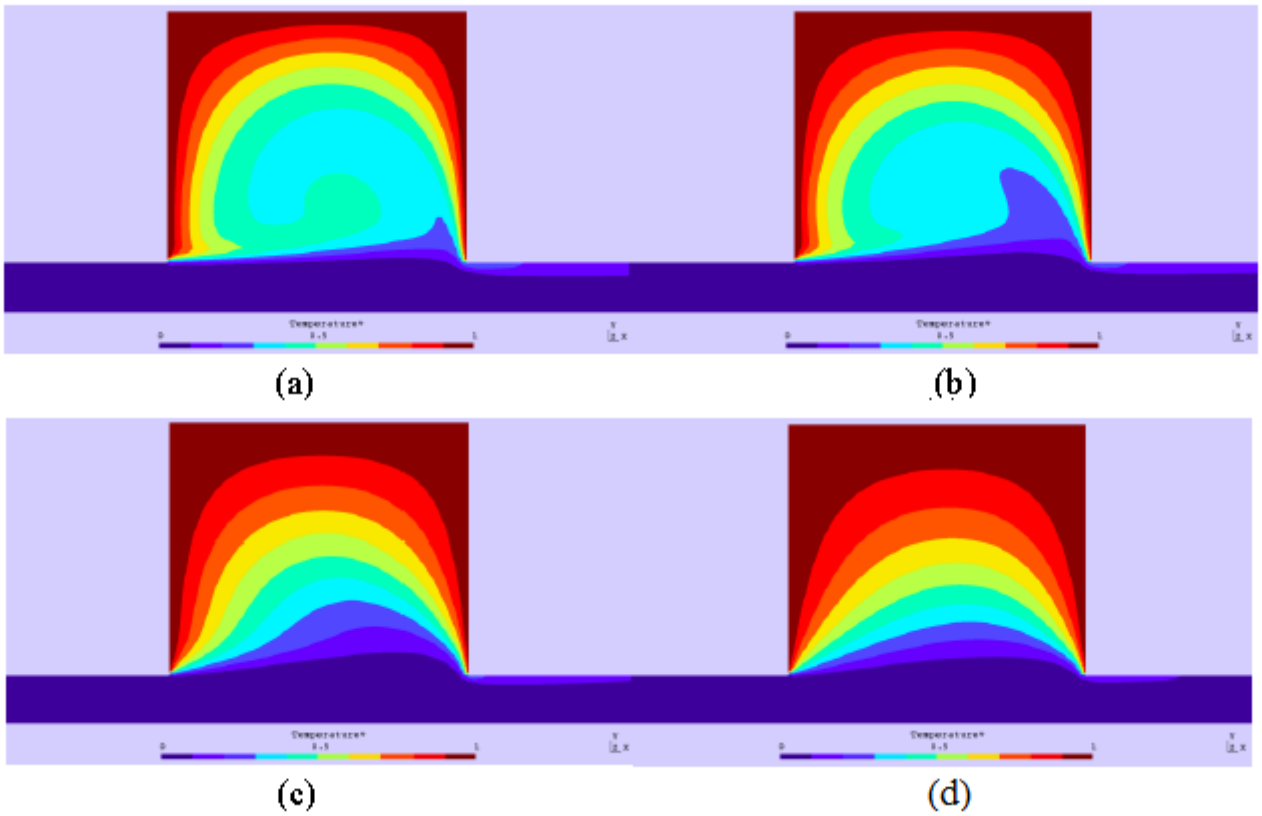

Figure 8. Temperature zones for different *Pl* number: (a) *Pl* = 0.083; (b) *Pl* = 0.233; (c) *Pl* = 0.380; (d) *Pl* = 0.796.

The behavior of the unyielded regions in the flow can be observed in Fig. 9. As the plastic number increases, the viscoplastic behavior increases too, and the unyielded regions begin to appear. It is possible to observe in Fig. 9 (d) the influence of the secondary flow: there is an unyielded region near the center of the vortex followed by a yielded zone in its boundaries. The profile created by the vortex begins to be restricted by the increase of the plastic number, which increases the unyielded regions and decreases the heat exchange capacity in the cavity. When the plastic number assumes a value between 0.437 and 0.449 the primary flow loses the capacity to induce the secondary flow. It is possible to observe that the cavity begins to have predominantly unyielded areas and the flow in the channel is influenced by the increase of the plastic number as well.

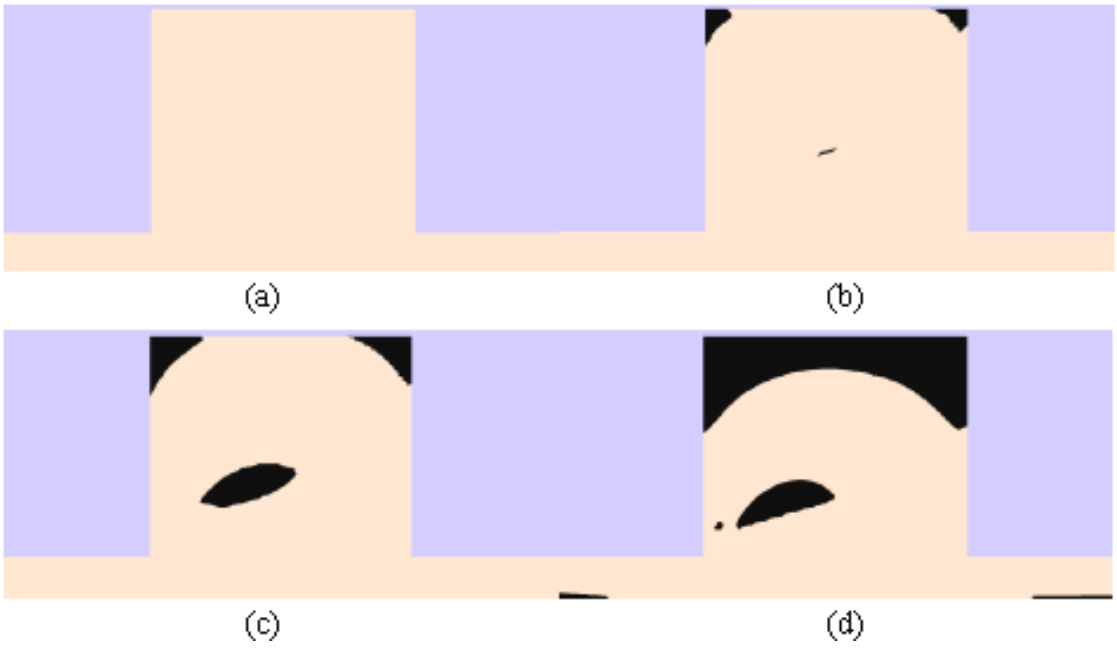

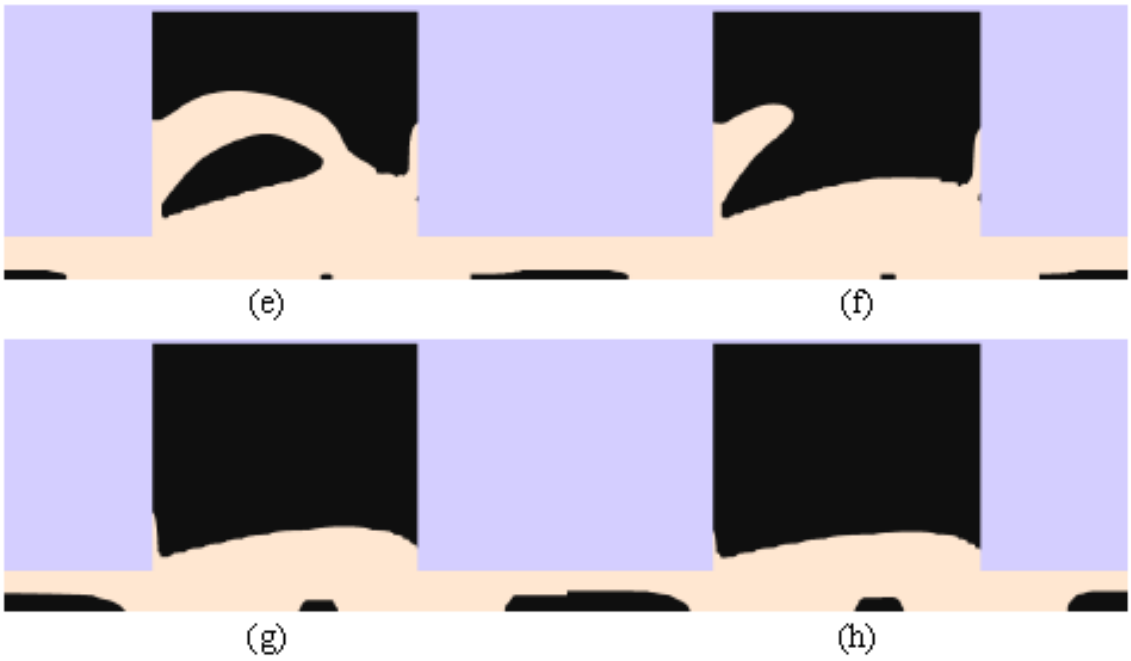

Figure 9. Yield zones for different Pl numbers: (a) *Pl* = 0.083; (b) *Pl* = 0.145; (c) *Pl* = 0.233; (d) *Pl* = 0.380; (e) *Pl* = 0.437; (f) *Pl* = 0.449; (g) *Pl* = 0.727; (h) *Pl* = 0.796.

Figure 10 shows the temperature profile along the geometry vertical centerline for different *Pl*. For low values of the plastic number, it is possible to identify the presence of a secondary flow, which in a first instance causes a rapid increase in temperature, followed by an almost constant temperature zone in the central region of the vortex, and then the temperature starts to rise again once the boundary of the vortex is achieved. With the increase of *Pl*, the unyielded zones increase their influence, and decrease the influence of the vortex, until the secondary flow becomes unfeasible. Because of the chosen *Re*, when the vortex is not present, the temperature starts to rise only when $y^* > H1$, in other words: the temperature only rises when y^* is bigger than the channel height. This happens because of the low heat transfer between the channel fluid and the cavity fluid.

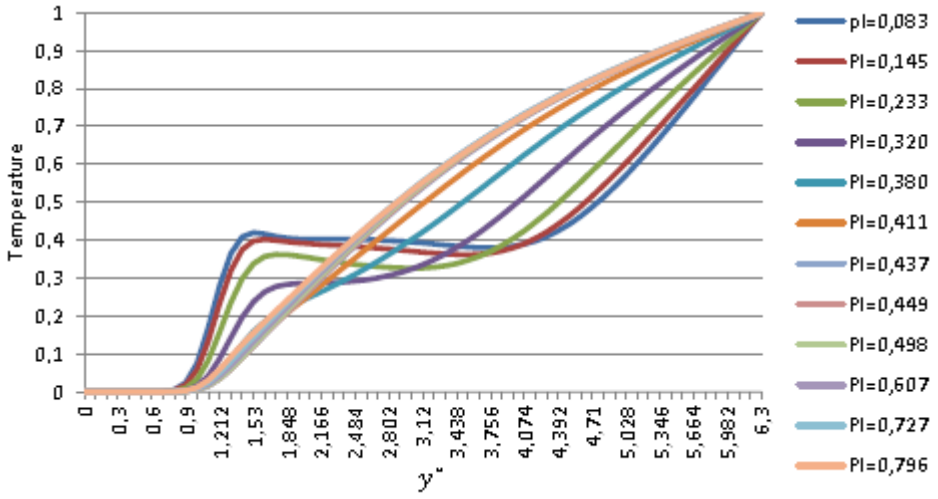

Figure 10. Temperature along the axis y^* for different *Pl.*

The temperature distribution at the wall of the downstream channel of the cavity is shown in Fig. 11. In this graph, it is possible to identify that with a lower *Pl*, the influence of the vortex increase, and the heat exchange provoked by it increases too, so the temperature downstream tends to be higher. Once inside the downstream channel, the walls are insulated, so the fluid tends to homogenize the temperature.

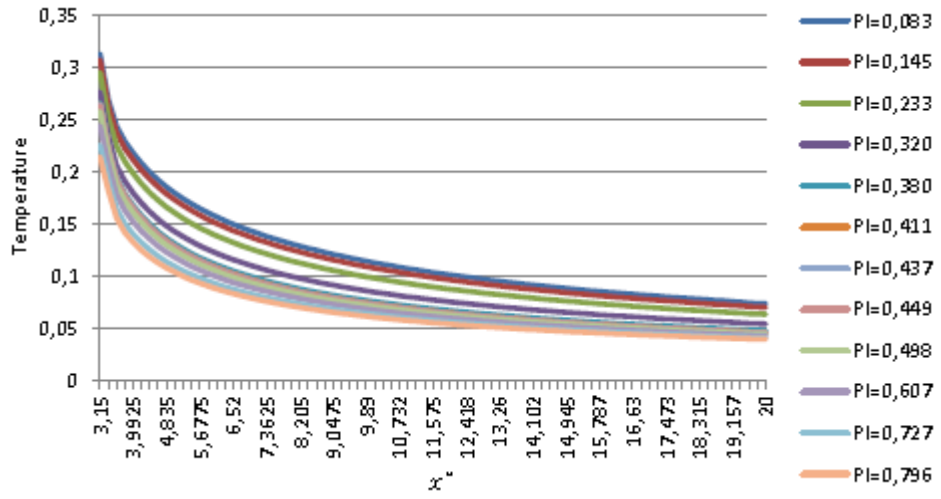

Figure 11: Temperature along the upper wall of the downstream channel for different *Pl.*

For low *Pl*, there are less unyielded regions and the secondary flow enhance the heat exchange by convection, and thus the average Nusselt tends to be higher. As the *Pl* increases, the rigid zones increase and the vortex influence decreases. This behavior can be seen in Fig. 12: up to *Pl* = 0.449 it is possible to identify the influence of the vortex, and the average Nusselt number curve as a function of *Pl* is decreasing. From *Pl* = 0.449, the curve continues to decrease but with a smaller slope, since now the Nusselt decreases only due to the increase of the unyielded region, as the vortex is no longer present.

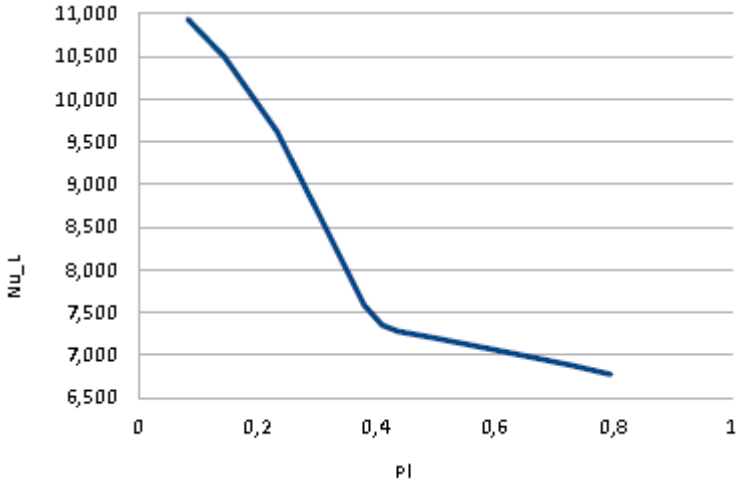

Figure 12. Average Nusselt number evaluated at the perimeter of the cavity as a function of the plastic number.

4. CONCLUSION

The Reynolds number variation, while maintaining the other dimensionless groups fixed, showed that for the studied range, the increase of Reynolds number decreases the thermal interaction of the channel with the cavity, but the increase of the Reynolds number also allows the arising of a secondary flow, that increases the heat exchange by convection and consequently increases the average Nusselt number. The increase of the Reynolds number also induced a loss in the temperature of the channel downstream of the cavity, due to the low interaction between the fluid parts that are in different areas of the geometry. The profile of the unyielded regions, showed the presence of a vortex within the cavity and that influences the distribution of the extra-stress for higher *Re*.

The increase of the plastic number decreases the thermal interaction capacity of the channel fluid with the cavity fluid. The increase of the plastic number restricts the flow due to the increase of the fluid yield stress with respect to the flow stress level and causes the increase of the rigid zones, decreasing the heat transfer by convection and decreasing the average Nusselt. The increase in the predominance of unyielded regions within the cavity also caused a decrease in the temperature of the channel wall downstream.

5. REFERENCES

de Souza Mendes, P. R., 2007. "Dimensionless non-Newtonian fluid mechanics". *Journal of Non-Newtonian Fluid Mechanics*, Vol. *147*, pp .109–116.

de Souza Mendes, P. R., and Dutra, E. S. S., 2004. "Viscosity function for yield-stress liquids". *Applied Rheology*, Vol. *14*, pp. 296–302.

Frigaard, I. A., Paso, K. G., and de Souza Mendes, P. R., 2017. "Bingham's model in the oil and gas industry". Rheologica Acta

Gupta, A. K., Mishra, P., and Chhabra, R. P., 2017a. " Momentum and heat transfer characteristics of a thin circular disk in Bingham plastic fluids" . Numerical Heat Transfer, Part A: Applications

Gupta, A. K., Gupta, S., and Chhabra, R. P., 2017b. "Natural convection in Bingham plastic fluids from an isothermal spheroid : Effects of fluid yield stress , viscous dissipation and temperature-dependent viscosity". Korea-Australia Rheology Journal, Vol. 29, pp. 163–184.

Hermany, L., 2012. *Aproximações estabilizadas de escoamentos de fluidos viscoplásticos através de uma expansão seguida de uma contração axissimétrica.* Master thesis, Universidade Federal do Rio Grande do Sul, Porto Alegre, Brazil.

Nirmalkar, N., Bose, A., and Chhabra, R. P., 2014. "Free convection from a heated circular cylinder in Bingham plastic fluid". International Journal of Thermal Sciences, 83, 33–44.

Nouar, C., Lebouché, M., Devienne, and Riou, C., 1995. "Numerical analysis of the thermal convection for Herschel-Bulkley fluids". International Journal of Heat and Fluid Flow, Vol. 13, pp. 223–232.

Raja, A. H., Patel, S. A., and Chhabra, R. P., 2015. "Laminar forced convection heat transfer from a two-dimensional transverse plate in Bingham plastic fluids". International Journal of Heat and Mass Transfer, Vol. 83, pp. 690–709.

Santos, D.D. , Furtado, G.M., Frey, S., Naccache, M.F., and de Souza Mendes, P.R., 2013. "Numerical investigation of elastic and viscous effects on inertial viscoplastic fluid flows*"*. In 2*2nd International Congress of Mechanical Engineering – COBEM2013*.

Santos, D.D. , Machado, L. G. S., 2015. "Numerical investigation of forced convection of non-newtonian fluids across a squere cylinder". In 2*3nd International Congress of Mechanical Engineering - COBEM2015*. Rio de Janeiro, Brazil.

Shyam, R., and Chhabra, R. P., 2013. "Effect of Prandtl number on heat transfer from tandem square cylinders immersed in power-law fluids in the low Reynolds number regime". International Journal of Heat and Mass Transfer, Vol. 57, pp. 742–755.

Soares, M., Naccache, M. F., and de Souza Mendes, P. R., 1999. "Heat transfer to viscoplastic materials flowing laminarly in the entrance region of tubes". International Journal of Heat and Fluid Flow, Vol. 20, pp. 60–67.

Turan, O., Poole, R. J., and Chakraborty, N., 2011. "Aspect ratio effects in laminar natural convection of Bingham fluids in rectangular enclosures with differentially heated side walls". Journal of Non-Newtonian Fluid Mechanics, 166(3–4), 208–230.

6. RESPONSIBILITY NOTICE

The authors are the only responsible for the printed material included in this paper.